STATISTICS, OPTIMIZATION AND INFORMATION COMPUTING
Stat., Optim. Inf. Comput., Vol. **x**, Month 202x, pp 0–19.
Published online in International Academic Press (www.IAPress.org)

Stability Analysis of Influenza Virus Spread Model in Bird Population with Reaction-Diffusion

M. Nur H. Qomarudin [1,2], Fatmawati [1,*], Windarto [1], Zviiteyi Chazuka [3]

[1] *Department of Mathematics, Faculty of Science and Technology, Universitas Airlangga, Surabaya 60115, Indonesia*
[2] *Department of Mathematics, Faculty of Exact Science, Universitas Nahdlatul Ulama Blitar, Blitar 66136, Indonesia*
[3] *Institute of Global Health, University College London, Gower Street, London WC1E 6BT, United Kingdom*

Abstract The avian influenza virus is a pathogen that predominantly infects wild birds but can also affect domestic poultry. This study established an epidemiological model, $SEIZ$, which incorporates infection factors from contaminated environments and transmission resulting from contact among avian species. The model was mathematically analyzed to identify two equilibrium points: a disease-free equilibrium point that is locally asymptotically stable when $\mathcal{R}_0 < 1$, indicating potential extinction of the bird, and an endemic equilibrium point that is locally asymptotically stable when $\mathcal{R}_0 > 1$, leading to disease persistence within the population. The model was subsequently transformed into a reaction-diffusion model featuring Gaussian initial conditions and Neumann boundary conditions. The developed reaction-diffusion model was subsequently solved numerically employing the finite volume method, utilizing parameters derived from empirical data. Simulation results indicated that an increase in the basic reproduction number can expedite viral infection. Moreover, augmenting the diffusion coefficient accelerates the propagation of infection into regions with the highest density of susceptible individuals and broadens the geographical extent. Virus concentrations in the environment exhibit longer persistence than those in infected populations, thereby increasing the probability of serving as a source of future infections. This study's findings suggest that control strategies for avian influenza virus should account for both direct and indirect infections, as well as the spatial movement of avian hosts, since such movement substantially affects virus spread and the efficacy of control measures.

Keywords Influenza, Mathematical model, Stability, Reaction-diffusion model, Finite volume method

AMS 2010 subject classifications 92B05, 65M08, 37N25

DOI: 10.19139/soic-2310-5070-3419

1. Introduction

The influenza A virus strain is the source of the avian influenza virus, which can infect domestic and wild birds and cause mild to severe illness [1]. More than 100 species of wild birds are known to be infected with the avian influenza A virus, which targets the respiratory and digestive systems of birds. Several natural hosts of avian influenza A that carry the virus include terns, gulls, coastal birds, and wild birds such as juvenile geese and ducks [2]. When birds come into contact with each other through dung, feathers, bedding, mucus, saliva, or other fluids, the influenza virus can spread [3]. Viral transmission occurs not only through direct contact with sick birds, but also through the environment. Similarly, several viruses found in the meat of infected birds can spread to vulnerable birds by consuming their corpses. The avian influenza A virus can spread through water or through lake sediments where aquatic birds are excreted, while its ability to survive in aquatic environments is still unclear [4].

*Correspondence to: Fatmawati (Email: fatmawati@fst.unair.ac.id). Department of Mathematics, Faculty of Science and Technology, Universitas Airlangga. Jalan Dr. Ir. H. Soekarno, Surabaya, East Java, Indonesia (60115).

ISSN 2310-5070 (online) ISSN 2311-004X (print)

The main hosts of the influenza A virus reservoir are wild birds. The seasonal movement of these birds increases the chance of a pandemic by giving the virus more opportunity to spread across geographically dispersed areas [5]. The highly pathogenic H5N1 virus was first found in wild birds near Lake Qianghia in 2005. Since then, the virus has spread throughout the world as a result of wild birds migrating [6]. Furthermore, in 2014, a highly pathogenic avian influenza virus was discovered in South Korea. In mid-2015, the virus expanded to Europe, Asia and possibly North America. In 2020, a number of European nations saw catastrophic outbreaks due to the spreading virus. Phylogenetic study suggests that this virus was brought from Africa by migratory birds [7]. In 2021, South Carolina's wild wigeon became infected with the HPAI H5N1 virus. According to a different study, a wave of 2,501 detections was recorded in 43 states and 91 distinct places in 2022. 8,001 cases were detected in the 48 US states and Alaska between August 2022 and mid-2023, marking another surge in this disease. During the seasonal avian migration between North and South America in the fall and spring, this case detection peaked [8].

The previously mentioned investigation of influenza virus propagation patterns necessitates a method that integrates temporal and geographical aspects. Various researchers have developed a number of mathematical models of influenza virus propagation based on a variety of factors and objectives. In his research, Misra employed the traditional SIR model to uncover a scenario of influenza virus transmission in which vaccination and quarantine could lower the virus's rate of spread [9]. In addition to lowering the rate of virus transmission, movement restrictions can also stop the spread of wild virus strains. The mathematical model of Kanyiri et al. shows a situation in which the movement restrictions put in place can also stop the spread of wild virus strains [10]. Concurrently, Tchuenche et al. presented a summary of the best ways to treat the virus while reducing expenses in their model [11]. These studies did not take spatial diffusion factors that could increase the virus's geographic reach, nor did they consider the risk of infection from birds and the environment.

Mathematical model of influenza virus propagation using diffusion parameters was presented by Zhang and Wang [12]. This model excludes environmental elements, which are a critical cause of influenza virus propagation, in favor of examining the presence of traveling waves. In a similar way, Xu and Ai [13] proposed a reaction-diffusion model of influenza virus transmission. As a study element, they were able to effectively explain the minimal speed necessary for a wave of viral dissemination. These observations offer general initial or boundary conditions that can be modified for this investigation to describe potential realistic scenarios . Additionally, Xu et al. proposed a model with three equations that can be applied to both human and animal populations; however, in order to understand disease dynamics in a particular population, the model must be simplified for a single species [14]. A mathematical model of influenza virus transmission in two populations—avian and human—with incidence effects and exposed classes in the avian population was presented by Khan et al. [15]. Consequently, investigating migratory factors in the model offers a chance for more observation. The model presented by Mu and Yang examined the dynamics of virus dissemination in two populations, taking into account the impacts of incidence and the existence of latent classes in the human population, all without taking environmental factors into account [16]. While the diffusion factor was not one of the characteristics of observation, the model observed by Malek A and Hoque A took into account environmental factors that can affect the number of transmissions that occur in the cattle environment [17]. A model incorporating diffusion was also presented by Tadmon et al., although they did not observe the exposed class in the avian population [18].

The objective of this investigation is to create a novel model for the transmission of influenza viruses in avian populations, which will enhance the body of existing research by introducing a number of fundamental innovations. The model developed in this study is an extension of the model presented by [15], which incorporates environmental transmission. The primary objective of this model is to investigate the manner in which the virus disseminates among avian populations in relation to environmental variables and avian spatial diffusion. This is achieved by employing a reaction-diffusion model that is constructed using Gaussian-distributed initial conditions. Each population is subjected to homogeneous Neumann boundary conditions in order to simulate an isolated domain in this investigation. This study additionally provides scenarios demonstrating the influence of avian movement and environmental factors on disease transmission, utilizing empirical data. The finite volume method is employed to simulate the established reaction-diffusion model, facilitating a thorough examination of the model's dynamics and the consequent diffusion effects. This study offers a theoretical framework to enhance the comprehension of diffusion's role in epidemiological dynamics and presents practical contributions that can serve as a reference for

interventions against influenza spread in avian populations. The influenza virus transmission model presented in Section 2 of this study, along with the positivity, boundedness, and positive invariance of the solution, is rigorously analyzed. Section 3 establishes the model's equilibrium point and basic reproduction number, while Section 4 presents a local asymptotic stability analysis. Section 5 illustrates the transmission of the disease by developing a reaction-diffusion model based on a real-world scenario. Section 5 employs the finite volume method to elucidate the derived solution of the reaction-diffusion model. Section 6 delineates numerical simulation outcomes derived from empirical data collected. Section 7 concludes this study and encapsulates our findings.

2. Mathematical Model

The model created in this work, which uses the bird population as its observational focus, is an expansion of the model examined in [15]. Environmental transmission elements, which are one of the reasons of transmission in the model shown in [18], will also be considered in this evaluation. The susceptible bird population $S(t)$, the exposed bird population $E(t)$, and the infected bird population $I(t)$ and the amount of viruses particle in the environment $Z(t)$ make up the four compartments of the model created in this study. This model explains the potential for transmission from the quantity of particle viruses in the environment as well as from contact between susceptible birds. In the context of the model that has been constructed, the model is presumed to be a closed population model that exclusively relies on the birth factor of vulnerable avians and does not account for avian recruitment through emigration. Complete information about the variables and parameters used is provided in Table 1.

Table 1. Influenza viral propagation model parameters and state variables

Influenza Virus Spread Model State Variables		
Symbol	Description	Unit
S	Susceptible bird population	Bird
E	Exposed bird population	Bird
I	Infected bird population	Bird
Z	Viral load in the environment	Virus particles
Influenza Virus Spread Model Parameters		
Symbol	Description	Unit
π	Bird population recruitment rate	Bird/day
γ	Environment-to-bird transmission rate	(Virus particle)$^{-1}$ day^{-1}
β	Bird-to-bird transmission rate	Bird^{-1} day^{-1}
μ	Natural mortality rate of birds	day^{-1}
α	Infection rate of exposed population	day^{-1}
υ	Virus shedding rate by infected birds	Virus particles/bird/day
ξ	Environmental viral clearance rate	day^{-1}

The formula for the study's total population at time t is $N(t) = S(t) + E(t) + I(t)$. Since vertical infection is not assumed by the model, every new bird added to the population is classified as healthy and joins the susceptible class at a rate of π. Observations about the presence of disease-related mortality or recovery are not provided because the model developed for this study does not presume the occurrence of an acute phase of the epidemic. Furthermore, susceptible birds will enter the Exposed class at rates β and γ as a result of contact with infected birds and various environmental viruses. Additionally, the birds in the exposed group will become infectious and enter the infected category at an average rate of α. In this case, natural mortality can occur in each population at a rate of μ. While natural or intentional clearance mechanisms can lower the amount of virus in the environment at an

average rate of ξ, infected birds are thought to shed the virus they carry at a rate of υ. In this instance, it is assumed that the virus's resistance in the environment is uniform and that the rate at which the virus degrades (naturally) is the same in every location. A compartment diagram used to illustrate the principles discussed is shown in Figure 1.

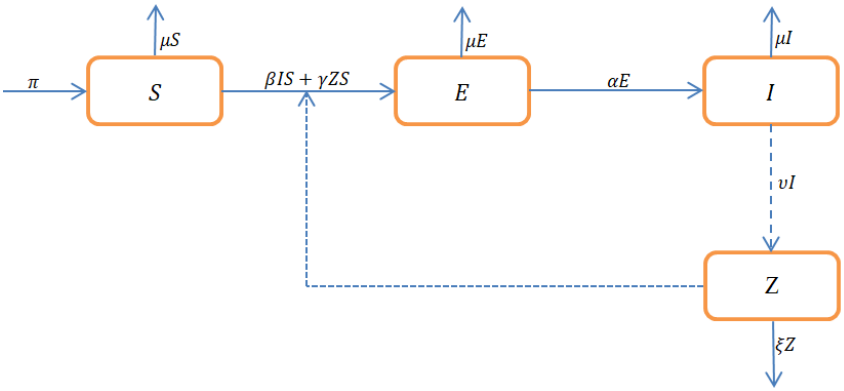

Figure 1. The compartment design for the model of influenza virus transmission

Equation (1) represents the influenza virus spread model used in this investigation as a nonlinear ordinary differential equation system.

$$\begin{aligned}
\frac{dS}{dt} &= \pi - \beta IS - \gamma ZS - \mu S,\\
\frac{dE}{dt} &= \beta IS + \gamma ZS - \alpha E - \mu E,\\
\frac{dI}{dt} &= \alpha E - \mu I,\\
\frac{dZ}{dt} &= \upsilon I - \xi Z.
\end{aligned} \tag{1}$$

with initial condition $S(0), E(0), I(0), Z(0) \geq 0$. If $t > 0$ is provided, equation (2)-(5) can be derived from equation (1) using non-negative initial conditions.

$$\begin{aligned}
S(t) = S(0)\exp\left(-\int_0^t (\beta I(\tau_1) + \gamma Z(\tau_1) + \mu)\, d\tau_1\right)\\
+ \pi \exp\left(-\int_0^t (\beta I(\tau_1) + \gamma Z(\tau_1) + \mu)\, d\tau_1\right)\int_0^t \exp\left(\int_0^\tau (\beta I(\tau_1) + \gamma Z(\tau_1) + \mu)\, d\tau_1\right) d\tau,
\end{aligned} \tag{2}$$

$$E(t) = E(0)e^{-(\alpha+\mu)t} + \int_0^t (\beta I(\tau) + \gamma Z(\tau))S(\tau)e^{(\alpha+\mu)(\tau-t)}\, d\tau, \tag{3}$$

$$I(t) = I(0)e^{-\mu t} + \alpha \int_0^t e^{\mu(\tau-t)}E(\tau)\, d\tau, \tag{4}$$

$$Z(t) = Z(0)e^{-\xi t} + \upsilon \int_0^t e^{\xi(\tau-t)}I(\tau)\, d\tau. \tag{5}$$

Equation (2) makes it evident that $S(t) \geq 0$. Clearly, $E(t), I(t), Z(t) \geq 0$ at (3)-(5) for $t = 0$. Consider $E(\tau), I(\tau), Z(\tau) \geq 0$ to be true for $\tau \in [0, t]$, $t > 0$. The next step will demonstrate that $E(t_1), I(t_1), Z(t_1) \geq 0$ hold for $t_1 > t$ (small) for $t_1 \in (t, t + \Delta t]$, allowing us to obtain (6)

$$I(t_1) = I(0)e^{-\mu t_1} + \alpha \int_0^{t_1} e^{\mu(\tau-t_1)}E(\tau)\, d\tau. \tag{6}$$

Consequently, it is evident that $I(t_1) \geq 0$. Therefore, it can be said that $I(t) \geq 0$. The equation $E(t), Z(t) \geq 0$ can be obtained by the same way. Thus, for time t, the solution of model (1) is positive invariant. Model (1) provides the whole dynamic form as follows:

$$\frac{dN}{dt} = \pi - \mu N. \tag{7}$$

Equation (7) can be integrated to get

$$N(t) = \frac{\pi}{\mu}\left(1 - e^{-\mu t}\right) + N(0)e^{-\mu t}. \tag{8}$$

If $t \to \infty$, then $\lim_{t\to\infty} N(t) = \frac{\pi}{\mu}$. Thus, it is possible to conclude that

$$0 \leq N(t) \leq \frac{\pi}{\mu}. \tag{9}$$

Equation (9) allows us to write the number of viruses in the environment in model (1) as equation (10).

$$\frac{dZ}{dt} + \xi Z \leq \frac{\pi\upsilon}{\mu}. \tag{10}$$

The integration result for equation (10) will give

$$Z(t) \leq Z(0)e^{-\xi t} + \left(1 - e^{-\xi t}\right)\frac{\pi\upsilon}{\mu\xi}. \tag{11}$$

Then, using equation (11), we get $\lim_{t\to\infty} Z(t) \leq \frac{\pi\upsilon}{\mu\xi}$ by taking $t \to \infty$. Consequently, the inequality (12) can be obtained.

$$Z(t) \leq \frac{\pi\upsilon}{\mu\xi}. \tag{12}$$

Based on the conclusions of equations (9) and (12), the solution set of system (1) is the closed set Ω, which is a finite set and positive invariant.

$$\Omega = \left\{(S, E, I, Z) \in \mathbb{R}^4 : N(t) \leq \frac{\pi}{\mu} \text{ and } Z(t) \leq \frac{\pi\upsilon}{\mu\xi}\right\}. \tag{13}$$

3. Stability Analysis of Steady States

In this chapter, the developed influenza virus transmission model in birds (1) will be used to calculate the equilibrium point. This section's computations yield two equilibrium points: the endemic fixed point and the disease-free fixed point. Furthermore, a detailed stability analysis of model (1) is given. By examining the derived eigenvalues, observations of the model's stability are made around the equilibrium point using the Jacobian matrix. When the disease spreads and $\mathcal{R}_0 > 1$, the endemic fixed point will be stable, and when $\mathcal{R}_0 < 1$, the disease-free fixed point will also remain stable.

3.1. Local Stability of Disease-Free Equilibrium

The initial step in finding this equilibrium point is to put $\frac{dS}{dt} = \frac{dE}{dt} = \frac{dI}{dt} = \frac{dZ}{dt} = 0$ in model (1). It is possible to obtain the disease-free equilibrium point when $E = I = 0$, which explains why susceptible birds do not become infected, i.e., $\mathbf{Q}_0 = \left(\frac{\pi}{\mu}, 0, 0, 0\right)$. Equation (14) is then used to calculate the basic reproduction number in the model (1) for the exposed, infected, and class Z populations using the next generation matrix.

$$\begin{pmatrix} \frac{dE}{dt} \\ \frac{dI}{dt} \\ \frac{dZ}{dt} \end{pmatrix} = F_a - V_a = \begin{pmatrix} \beta IS + \gamma ZS \\ 0 \\ 0 \end{pmatrix} - \begin{pmatrix} \alpha E + \mu E \\ -\alpha E + \mu I \\ -\upsilon I + \xi Z \end{pmatrix}. \tag{14}$$

Using equation (14) and the disease-free equilibrium point that was found, the nonnegative new infection matrix $\mathcal{F}_A$ and the disease transition matrix $\mathcal{V}_A$ are produced, specifically

$$\mathcal{F}_A = \begin{pmatrix} 0 & \beta\frac{\pi}{\mu} & \gamma\frac{\pi}{\mu} \\ 0 & 0 & 0 \\ 0 & 0 & 0 \end{pmatrix}, \quad \mathcal{V}_A = \begin{pmatrix} \alpha+\mu & 0 & 0 \\ -\alpha & \mu & 0 \\ 0 & -\upsilon & \xi \end{pmatrix}. \tag{15}$$

The spectral radius $\rho(\mathcal{F}_A\mathcal{V}_A^{-1})$ in equation (15) may be used to derive the basic reproduction number, which allows us to obtain the following equation

$$\mathcal{R}_0 = \frac{\alpha\pi(\beta\xi+\gamma\upsilon)}{(\alpha+\mu)\mu^2\xi}. \tag{16}$$

Theorem 1. *Let a disease-free fixed point* $\mathbf{Q}_0 = \left(\frac{\pi}{\mu}, 0, 0, 0\right)$ *in model (1), the disease-free fixed point will be locally Asymptotically stable if* $\mathcal{R}_0 < 1$.

Proof

To perform the stability analysis of disease-free fixed point in model (1), The Jacobian matrix evaluated at equilibrium point $\mathbf{Q}_0$ is:

$$J(\mathbf{Q}_0) = \begin{pmatrix} -\beta I - \gamma Z - \mu & 0 & -\beta S & -\gamma S \\ \beta I + \gamma Z & -\alpha-\mu & \beta S & \gamma S \\ 0 & \alpha & -\mu & 0 \\ 0 & 0 & \upsilon & -\xi \end{pmatrix}. \tag{17}$$

The characteristic equation $\det(J(\mathbf{Q}_0) - \lambda\mathbf{I}) = 0$ can be produced by substituting the disease-free equilibrium point in equation (17), resulting polynomial in (18) and the eigenvalue $\lambda_1 = -\mu < 0$

$$\lambda^3 + a_1\lambda^2 + a_2\lambda + a_3 = 0, \tag{18}$$

with

$$\begin{aligned} a_1 &= (\xi + 2\mu + \alpha), \\ a_2 &= (\alpha+\mu)(\xi+\mu) + \mu\xi - \frac{(\alpha+\mu)\beta\mu\xi}{(\beta\xi+\gamma\upsilon)}\mathcal{R}_0, \\ a_3 &= (1-\mathcal{R}_0)(\alpha+\mu)\mu\xi. \end{aligned} \tag{19}$$

As explained in [19], the Routh-Hurwitz criteria can be used to obtain the stability analysis in (18) in such a way that $a_1, a_3 > 0$ and $a_1a_2 - a_3 > 0$. Here, the following points are relevant:

(K1) Clearly $a_1 > 0$,

(K2) For $a_3 > 0$ then $\mathcal{R}_0 < 1$,

(K3) For $a_1a_2 - a_3 > 0$ will satisfies if $\mathcal{R}_1 < 1$ with

$$\mathcal{R}_1 = \frac{(\xi+2\mu+\alpha)\frac{\alpha\beta\pi}{\mu}}{(\alpha+\mu)(\xi+\mu)(\xi+2\mu+\alpha) + \mu\xi(\xi+\mu) + (\alpha+\mu)\mu\xi R_0}.$$

The third condition states that

$$\mathcal{R}_0 - \mathcal{R}_1 = \frac{\left(\frac{\alpha\pi\gamma\upsilon}{\mu^2} + \frac{\alpha\pi\gamma\upsilon}{\mu\xi} + \frac{\alpha\pi\beta\xi}{\mu^2}\right)(\xi+2\mu+\alpha) + \mu\xi(\xi+\mu) + (\alpha+\mu)\mu\xi R_0}{(\alpha+\mu)(\xi+\mu)(\xi+2\mu+\alpha) + \mu\xi(\xi+\mu) + (\alpha+\mu)\mu\xi R_0}, \tag{20}$$

Thus, it is clear that $\mathcal{R}_0 - \mathcal{R}_1 > 0$.

Hence, as the observations in (K1)-(K3) show, $a_1, a_2, a_3 > 0$ and model (1) is stable when $\mathcal{R}_0 < 1$ for the disease-free equilibrium point.

□

3.2. Local Stability of Endemic Equilibrium

In the steady state condition $\frac{dS}{dt} = \frac{dE}{dt} = \frac{dI}{dt} = \frac{dZ}{dt} = 0$ of equation (1), the endemic equilibrium point $\mathbf{Q}_1 = (S^*,\ E^*,\ I^*,\ Z^*)$ can be found when $E \neq 0$ and $I \neq 0$. This point indicates the occurrence of disease spread with

$$\begin{aligned} I^* &= \frac{\mu\xi}{(\beta\xi+\gamma\upsilon)}(\mathcal{R}_0 - 1), \\ E^* &= \frac{\mu^2\xi}{\alpha(\beta\xi+\gamma\upsilon)}(\mathcal{R}_0 - 1), \\ S^* &= \frac{\mu\xi(\alpha+\mu)}{\alpha(\beta\xi+\gamma\upsilon)}, \\ Z^* &= \frac{\upsilon\mu\xi}{\xi(\beta\xi+\gamma\upsilon)}(\mathcal{R}_0 - 1). \end{aligned} \tag{21}$$

For $I^* > 0$, we can obtain $\frac{\mu\xi}{(\beta\xi+\gamma\upsilon)}(\mathcal{R}_0 - 1) > 0$ using the equation (21). This indicates that $\mathcal{R}_0 > 1$, which ensures the spread of disease in birds.

Theorem 2. *Let an endemic fixed point* $\mathbf{Q}_1 = (S^*, E^*, I^*, Z^*)$ *in model* (1)*, the endemic fixed point will be locally Asymptotically stable if* $\mathcal{R}_0 > 1$.

Proof

In order to analyze the stability at the endemic fixed point $\mathbf{Q}_1$, the Jacobian matrix evaluated at endemic equilibrium point is

$$J(\mathbf{Q}_1) = \begin{pmatrix} -\beta I - \gamma Z - \mu & 0 & -\beta S & -\gamma S \\ \beta I + \gamma Z & -\alpha - \mu & \beta S & \gamma S \\ 0 & \alpha & -\mu & 0 \\ 0 & 0 & \upsilon & -\xi \end{pmatrix}. \tag{22}$$

The characteristic equation $\det(J(\mathbf{Q}_1) - \lambda\mathbf{I}) = 0$ in endemic equibrilium point allows us to find the eigenvalue $\lambda = -\mu$ and the polynomial (23).

$$A_3 + A_2\lambda + A_1\lambda^2 + \lambda^3 = 0, \tag{23}$$

with

$$\begin{aligned} A_1 &= \mu\mathcal{R}_0 + \mu + \xi + \alpha, \\ A_2 &= \mu\mathcal{R}_0(\xi + \alpha + \mu) + \left(\frac{1}{\beta\mu} - \frac{1}{(\beta\xi+\gamma\upsilon)}\right)\beta\mu(\alpha+\mu)\xi, \\ A_3 &= \mu\xi(\alpha+\mu)(\mathcal{R}_0 - 1). \end{aligned} \tag{24}$$

The Routh-Hurwitz criterion is also used to perform stability analysis at the endemic equilibrium point based on equation (23) using the same methodology as previously. In this instance, more computations are performed on (24), leading to

(KK 1) Clearly $A_1 > 0$,

(KK 2) For $A_3 > 0$ then $\mathcal{R}_0 > 1$,

(KK 3) For $A_1A_2 - A_3 > 0$ will hold if $\mathcal{R}_2 > 1$ with

$$\mathcal{R}_2 = \frac{\mu R_0 n_1(\mu R_0 + n_1) + (\mu+\alpha)n_1\xi + \mu\xi(\mu+\alpha)}{\frac{\beta\mu}{(\beta\xi+\gamma\upsilon)}(\mu+\alpha)\xi(\mu R_0 + n_1)}, \tag{25}$$

where:

$$n_1 = \mu + \xi + \alpha.$$

The third condition (KK3) ensures that $\mathcal{R}_2 - \mathcal{R}_0 > 0$ with

$$R_2 - R_0 = \frac{(\xi\mu R_0 + \frac{\alpha\pi\gamma\upsilon}{\mu\xi})(\mu R_0 + n_1) + (\mu+\alpha)n_1\xi + \mu\xi(\mu+\alpha)}{\frac{\beta\mu}{(\beta\xi+\gamma\upsilon)}(\mu+\alpha)\xi(\mu R_0 + n_1)}. \tag{26}$$

Thus, from (KK 1)-(KK 3), it is clear that when $\mathcal{R}_0 > 1$, the endemic equilibrium point will be in a locally asymptotically stable. □

3.3. Sensitivity Analysis

In order to guarantee that the model is applicable to the real world, factual data gathered from multiple sources will be incorporated into the final model construction. This data collection makes it possible to calibrate the model more precisely, which leads to more applicable and focused sensitivity analyses. A study by [20] estimated that the recruitment rates of the bird species common eiders (*Somateria mollissima*), which typically inhabit shallow beaches, range from 0.1 to $0.2\,\text{year}^{-1}$. Using spring stopover data from 2005 to 2015 in Delaware Bay, the United States, Tucker et al. reported conservation results on the red knot (Calidris canutus rufa), estimating recruitment rates for this bird species to be 0.088 $year^{-1}$ [21]. An experimental study by Bouma estimated that the average virus transmission rate from bird-to-bird contact is $0.44 - 1.3$/day [22]. In his research, Ssematimba offered a higher estimate of 2.3–4.3/day [23]. The biological characteristics of the objects under study are obviously the basis for this discrepancy. However, in order to cover the previously obtained results, the estimated range used in this study was $0.44 - 4.3$/day. According to Newton, the mortality rates of migratory birds vary by migration season, ranging from 5% to 93% for every three-month annual migration period [24].

The average number of wild birds infected by the disease is $0.28 - 1.28$ /day [25]. Based on a study by [26] that describes the abiotic factors of influenza virus resistance in aquatic bird habitats, this study used parameter value estimates for the range of virus clearance rates in the environment. The estimated value of virus clearance used in this study is $1/19.2 - 1/1.6$ particles virus/day. Specific data were not found for avian-environmental transmission rate; however, according to [27], there is a strong correlation between the number of infected birds and $30.9\% - 46.5\%$ of the amount of virus in the environment, indicating that environmental virus transmission cannot be ignored. According to [28], bird markets have a 38.1–56.5 % environmental virus exposure, while non-market areas have a lower 0.6–30.7 % exposure. The average risk of airborne influenza transmission is 9–58 $\%/\text{d}$ [29]. Thus, *avian-environmental transmission rate* will be assumed to be 0.1–$0.9/\text{d}$ in this study. The report of Germeraad et al. (2019), which examined the capacity of influenza virus shedding in avian species, both from the respiratory tract and cloacal tract of several avian species, with a shedding time of 0.3–$40.2\,\text{d}$, served as the basis for the estimated influenza virus emission rate in this study. Therefore, during that period, avian species can release 1–$6.5\,\log_{10}\text{EID}_{50}/\text{mL}$ [30]. Based on the references found, Table 2 lists the range of parameter values used in this investigation.

Table 2. Influenza Virus Transmission Model Parameter Values

Parameter	Value Range	Reference
π	0.088–0.22 $1/\text{yr}$	[20, 21]
γ	0.1–0.9 $1/\text{d}$	[27, 28, 29]
β	0.44–4.3 $1/\text{d}$	[22, 23]
μ	(0.05–0.93)/90 $1/\text{d}$	[24]
α	0.28–1.28 $1/\text{d}$	[25]
υ	1–6.5 $\log_{10}(\text{EID}_{50})/\text{mL}$ per 0.3–40.2 d	[30]
ξ	(1/19.2)–(1/1.6) $1/\text{d}$	[26]

Controlling the spread of disease requires an understanding of how it can penetrate a population in a particular location. Therefore, the sensitivity analysis of each parameter in the (1) model will be performed on the obtained

basic reproduction number in this subchapter. The purpose of this analysis is to identify the factors that contribute most to the disease's spread.

Model (1)'s parameters affect the basic reproduction number in different sensitivities. Afterwards, a sensitivity analysis will be presented to quantify the impact of every parameter on the basic reproduction number using the formula in [31], specifically

$$\chi_\tau = \frac{\partial \mathcal{R}_0}{\partial \tau} \cdot \frac{\tau}{\mathcal{R}_0}, \tag{27}$$

where χ_τ is the sensitivity index, $\mathcal{R}_0$ is the reproduction number, and τ is the parameter of interest. The sensitivity index calculations, based on the formula in (27), indicate that only the parameters μ and ξ have a negative effect on the $\mathcal{R}_0$ number. This implies that the basic reproduction number value will decrease with a higher value for this parameter.

In this instance, increasing a parameter with a positive sensitivity index raises the basic reproductive number. As illustrated in figure 2, the sensitivity index for the basic reproductive number is computed using parameter values: $\pi = 0.088/365$, $\gamma = 0.45$, $\beta = 0.443$, $\mu = 0.9/90$, $\alpha = 0.52$, $\upsilon = 0.017$, and $\xi = 1/19$. The basic reproductive number increases or decreases by 7.5% for every 10% increase or decrease in the transmission rate brought on by bird-to-bird contact. Meanwhile, the environment's average rate of transmission can influence the basic reproductive number's growth or decline by 2.47%.

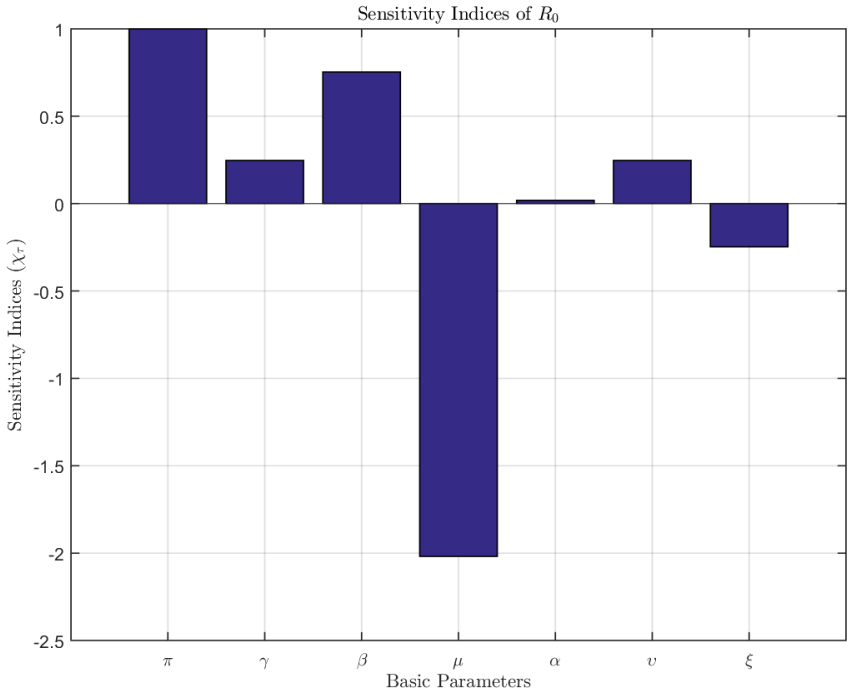

Figure 2. Sensitivity index of basic reproduction number

4. Diffusion Model

Avian influenza viruses are usually transmitted by bird-to-bird contact. The movement of birds, whether naturally occurring or as a result of human activity, can cause this spread to start in one area and then spread to other places. Influenza viruses are spread to humans through the secretions of the respiratory and digestive systems of domestic

birds [32]. As a result, this chapter will present the reconstruction of the model (1) in relation to the diffusion factors provided for each population to discuss the dynamics of influenza virus spread due to spatial movement. Assume $x \in \mathbb{R}$ is a restricted space domain that contains avian habitat. It is assumed that a bird's ability to move, either naturally or on not, allows disease to spread throughout the space domain. The number of susceptible, exposed, and infected birds as well as the number of viruses in the environment at x and time t will be represented in $S(x,t), E(x,t), I(x,t)$, and $Z(x,t)$. According to [33], the reaction-diffusion model in model (1) can be expressed as

$$\begin{cases} \dfrac{\partial S}{\partial t} = D_S \dfrac{\partial^2 S}{\partial x^2} + \pi - \beta IS - \gamma ZS - \mu S, \\ \dfrac{\partial E}{\partial t} = D_E \dfrac{\partial^2 E}{\partial x^2} + \beta IS + \gamma ZS - \alpha E - \mu E, \\ \dfrac{\partial I}{\partial t} = D_I \dfrac{\partial^2 I}{\partial x^2} + \alpha E - \mu I, \\ \dfrac{\partial Z}{\partial t} = D_Z \dfrac{\partial^2 Z}{\partial x^2} + \upsilon I - \xi Z, \end{cases} \tag{28}$$

with $x \in [-L_x, L_x]$ km as the spatial domain. We construct this model assuming that the birds move randomly in the desired area. For each population, the diffusion factors D_S, D_E, D_I, and D_Z in (km/day) are constant.

This study incorporates initial conditions that account for the spatial heterogeneity of susceptible avian populations in order to present a more realistic illustration. In particular, it is presumed that susceptible avian populations are concentrated in central habitats, such as water sources or feeding areas, where birds tend to congregate. This condition is represented as a Gaussian initial condition with a decreasing density as the domain boundary approaches. As stated in [34], the initial conditions adopted in the reaction-diffusion model in this study are stated as follows

$$\begin{cases} S(x,0) = S_0 \exp\left(-\dfrac{(x-x_c)^2}{\delta^2}\right), \\ E(x,0) = 0, \\ I(x,0) = I_0 \exp\left(-\dfrac{(x-x_i)^2}{\delta_i^2}\right), \\ Z(x,0) = \upsilon I_0 \exp\left(-\dfrac{(x-x_i)^2}{\delta_i^2}\right). \end{cases} \tag{29}$$

The center of the flock is defined as $x_c \in (-L_x, L_x)$ in the equation (29), where the spatial distribution of the susceptible population in this region is regulated by the parameter δ (in km). Additionally, the exposed avian population is initially zero at each location, with the infected population being localized at the outbreak center at position x_i, which is Gaussian-distributed where I_0 represents the peak initial infected density at the outbreak center. The viral load in this initial condition is subsequently proportionally scaled to the mean υ and distributed in accordance with the initial condition of the infected population. In this instance, the parameter δ_i (in km) denotes the spatial distribution of the infected population.

Additionally, the study implemented homogeneous Neumann boundary conditions with null flux across all compartments within each domain boundary. The adopted boundary conditions were implemented to examine the spatial dynamics of infection propagation within a region, disregarding the effects of population migration or

external infection sources. According to [35, 36], this boundary condition is mathematically expressed as follows:

$$\begin{cases} \left.\dfrac{\partial S}{\partial x}\right|_{x=-L_x} = \left.\dfrac{\partial S}{\partial x}\right|_{x=L_x} = 0, \\ \left.\dfrac{\partial E}{\partial x}\right|_{x=-L_x} = \left.\dfrac{\partial E}{\partial x}\right|_{x=L_x} = 0, \\ \left.\dfrac{\partial I}{\partial x}\right|_{x=-L_x} = \left.\dfrac{\partial I}{\partial x}\right|_{x=L_x} = 0, \\ \left.\dfrac{\partial Z}{\partial x}\right|_{x=-L_x} = \left.\dfrac{\partial Z}{\partial x}\right|_{x=L_x} = 0. \end{cases} \tag{30}$$

The boundary condition (30) demonstrates that there is no inward or outward migration within the observation area; thus, the source of infection is exclusively determined by local infection as indicated by equation (29). Thus, this boundary condition signifies a state of demographic isolation within the study area. This method allows for the analysis of virus transmission without accounting for external factors [37].

5. Finite Volume Scheme

In order to solve model (28) numerically, the finite volume approach will be applied with the specified domain. According to [38], the one-dimensional volume integration of equation (28) in a susceptible population, which produces

$$\int_{\Delta V} \frac{\partial S}{\partial t}\,\mathrm{d}V = \int_{\Delta V} D_S \frac{\partial^2 S}{\partial x^2}\,\mathrm{d}V + \int_{\Delta V} (\pi - \beta I S - \gamma Z S - \mu S)\,\mathrm{d}V\,. \tag{31}$$

According to the divergence theorem, the volume integral is transformed into a surface flux. Additionally, given the center points of the West (W), East (E), and Central (P) surface control volumes, the volume integral for the right-hand side of equation (31) with respect to the diffusion term yields the following expression.

$$\int_{\Delta V} D_S \frac{\partial^2 S}{\partial x^2}\,\mathrm{d}V = D_S \left[\left(\frac{\partial S}{\partial x}\right)_e - \left(\frac{\partial S}{\partial x}\right)_w \right], \tag{32}$$

where e and w denote the east and west surfaces of the control volume, respectively. The gradient of the cell

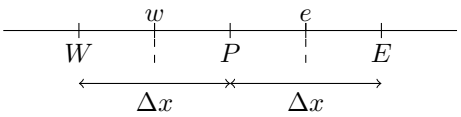

Figure 3. Control volume with center points W, P, E and surfaces w and e

surface is estimated through linear interpolation at the nearest cell center with a uniform grid spacing of Δx as in Figure 3, specifically:

$$\left(\frac{\partial S}{\partial x}\right)_e \approx \frac{S_E - S_P}{\Delta x} = \frac{S_{i+1,j} - S_{i,j}}{\Delta x}, \quad \left(\frac{\partial S}{\partial x}\right)_w \approx \frac{S_P - S_W}{\Delta x} = \frac{S_{i,j} - S_{i-1,j}}{\Delta x}. \tag{33}$$

Inserting the equation (33) into (32) yields a discretisation of the diffusion formula as follows:

$$\int_{\Delta V} D_S \frac{\partial^2 S}{\partial x^2}\,dV = D_S \left(\frac{S_{i+1,j} - 2S_{i,j} + S_{i-1,j}}{\Delta x} \right). \tag{34}$$

In the reaction formula on the right-hand side of equation (31), discretisation is executed utilising the cell-centered surface method, where these values denote the average values within the control volume, yielding

$$\begin{aligned}\int_{\Delta V} (\pi - \beta IS - \gamma ZS - \mu S)\, dV &= (\pi - \beta I_P S_P - \gamma Z_P S_P - \mu S_P)\, \Delta x \\ &= (\pi - \beta I_{i,j} S_{i,j} - \gamma Z_{i,j} S_{i,j} - \mu S_{i,j})\, \Delta x. \end{aligned} \tag{35}$$

Nonetheless, the implicit and explicit Euler methods applied to the volume integral on the left-hand side of (31) yield the subsequent outcome.

$$\int_{\Delta V} \frac{\partial S}{\partial t}\, \mathrm{d}V = \frac{\partial S}{\partial t} \Delta x \approx \frac{S_{i,j+1} - S_{i,j}}{\Delta t} \Delta x. \tag{36}$$

Based on the outcomes of equations (31)- (36), it can be inferred that

$$\begin{aligned} S_{i,j+1} = S_{i,j} &+ D_S \left(\frac{S_{i+1,j} - 2S_{i,j} + S_{i-1,j}}{\Delta x^2} \right) \Delta t \\ &+ (\pi - \beta I_{i,j} S_{i,j} - \gamma Z_{i,j} S_{i,j} - \mu S_{i,j})\, \Delta t, \end{aligned} \tag{37}$$

where the indices i, j correspond to the spatial position x and the temporal position t, respectively. In the finite volume scheme, the outside node substitution is used to guarantee that the flux and solution continuously satisfy the boundary conditions. At the domain boundary $x = -L_x$, the control volume that aligns with the boundary is null, as indicated in equation (30). According to the boundary conditions, the flux value on the west surface w is given by $\left(\frac{\partial S}{\partial x}\right)_w = 0$. The volume integral of the diffusion term (32) is expressed as follows:

$$\int_{\Delta V} D_S \frac{\partial^2 S}{\partial x^2} dV = D_S \left[\left(\frac{\partial S}{\partial x} \right)_e - \underbrace{\left(\frac{\partial S}{\partial x} \right)_w}_{=0} \right] = D_S \left(\frac{\partial S}{\partial x} \right)_e \approx D_S \frac{S_E - S_P}{\Delta x}. \tag{38}$$

For the center of the control volume P at spatial position $i = 1$, the following equation is applicable.

$$\int_{\Delta V} D_S \frac{\partial^2 S}{\partial x^2} dV = D_S \left(\frac{S_{2,j} - S_{1,j}}{\Delta x} \right). \tag{39}$$

Inserting the equation (39) into (37) will yield

$$S_{1,j+1} = S_{1,j} + \frac{D_S \Delta t}{(\Delta x)^2} (S_{2,j} - S_{1,j}) + (\pi - \beta I_{1,j} S_{1,j} - \gamma Z_{1,j} S_{1,j} - \mu S_{1,j})\, \Delta t, \tag{40}$$

which represents the volume integral of the diffusion term at $x = -L_x$. Additionally, at the right boundary $x = L_x$, the condition $\left(\frac{\partial S}{\partial x}\right)_e = 0$ holds, allowing us to derive the following equation:

$$\int_{\Delta V} D_S \frac{\partial^2 S}{\partial x^2} dV = D_S \left[\underbrace{\left(\frac{\partial S}{\partial x} \right)_e}_{=0} - \left(\frac{\partial S}{\partial x} \right)_w \right] = -D_S \left(\frac{\partial S}{\partial x} \right)_w \approx -D_S \frac{S_P - S_W}{\Delta x}. \tag{41}$$

Substituting the equation (41) into (37) for the spatial position $i = N$ yields

$$\int_{\Delta V} D_S \frac{\partial^2 S}{\partial x^2} dV = -D_S \left(\frac{S_{N,j} - S_{N-1,j}}{\Delta x} \right) = D_S \left(\frac{S_{N-1,j} - S_{N,j}}{\Delta x} \right). \tag{42}$$

The final step in addressing this boundary condition is to substitute the diffusion term in equation (37) with the volume integral at the boundary $x = L_x$ from equation (42) to produce

$$S_{N,j+1} = S_{N,j} + \frac{D_S \Delta t}{(\Delta x)^2} \left(S_{N-1,j} - S_{N,j}\right) + \left(\pi - \beta I_{N,j} S_{N,j} - \gamma Z_{N,j} S_{N,j} - \mu S_{N,j}\right) \Delta t. \tag{43}$$

The numerical methods for the populations E, I, and Z are derived by employing the same procedures as outlined in equations (31)-(42). Next, to guarantee the stability and precision of the simulation, the Courant-Friedrichs-Lewy stability condition, as referenced in [39, 34], is employed and is expressed by the subsequent formula

$$\Delta t \leq \frac{(\Delta x)^2}{2 \max(D_S, D_E, D_I, D_Z)}. \tag{44}$$

The dimensional grid size employed is $\Delta x = 0.05$ km, accompanied by a time grid of $\Delta t = 0.01$, thereby satisfying the condition outlined in formula (44). The finite volume scheme described above will be applied to analyze the spatial spreading of avian influenza in the subsequent chapter.

6. Numerical Results

The reaction-diffusion model of influenza virus spread (28) employs numerical simulations grounded in empirical data from chapter 3.3 to depict a more realistic scenario of influenza virus dissemination. This study depicts the avian movement trajectory within the spatial domain $x \in [-5, 5]$ km, corresponding to an avian distribution area of 10 km. The parameter $\delta = \delta_i = 0.1 \times L_x = 2$ km denotes the radius of the population distribution at the outbreak center and the locus of the susceptible avian population. The boundary conditions employed in this simulation are specified in equation (30), which delineates the domain's boundary that is insulated from external influences. The specified boundary conditions suggest that there is no avian migration or infection that transcends regional limits; thus, the dynamics of virus movement and dissemination are solely attributable to interactions among avians within the observed area. The infection source is solely derived from the initial outbreak within the infected population and the viral load present in the environment. The numerical implementation of the reaction-diffusion model (28), incorporating Neumann boundary conditions, is resolved utilizing the finite volume method as delineated in formulas (37)-(44). The resultant simulation is depicted in Figure 4 for $\mathcal{R}_0 > 1$ and in Figures 5 to 6 for $\mathcal{R}_0 < 1$. The diffusion coefficient employed in the simulations was augmented in Figure 6 to assess the impact of spatial diffusion on the dynamics of disease propagation.

Several fundamental scenarios are varied in this simulation to elucidate the interaction between epidemiological parameters and spatial movement. As illustrated in Figure 4, the initial scenario employs low diffusion, which is indicative of a high transmission rate in the population, with $\mathcal{R}_0 > 1$. For $\mathcal{R}_0 < 1$, the second scenario is illustrated in Figure 5, which illustrates conditions in which local transmission is relatively low. In order to examine the dynamics of virus spread against an increased diffusion coefficient, the third scenario, illustrated in Figure 6, employs the same parameter values as the second scenario, but with an increased diffusion coefficient value that reflects the population's freer movement. The parameter values utilized in this simulation are displayed in Table 2 to ensure a realistic simulation. Based on empirical data that accurately represents a realistic outbreak, the parameters were chosen for the scenario in which $\mathcal{R}_0 > 1$. In order to ensure that $\mathcal{R}_0 < 1$, the assumption of $\beta = 0.2$ is made for basic reproduction numbers that are below the epidemiological threshold.

The spatial profile of the susceptible population for $\mathcal{R}_0 > 1$ is depicted in Figure 4a. The susceptible population is Gaussian distributed with a density center at $x = 0$ km at the initial condition of $t = 0$ days. This population experiences a decrease in size over time as a result of spatially occurring infections. The peak of infections at $x = 0$ km is concurrent with the decline in the susceptible population, which occurs only in 12 days around $x = -1$ km. The simulation results accurately illustrate the temporal and spatial correlation between the increase in the number of infected avians and the decline in the susceptible avian population. In the second scenario, the susceptible population experiences a substantial decline only 21 days after the outbreak. This suggests that the rate of infection spread is slower when local transmission is lower. In contrast, Figure 6a displays more intriguing findings in the

third scenario. Despite the fact that $\mathcal{R}_0 < 1$, the susceptible population experienced a substantial decline within 11 days of the outbreak, which was significantly faster than in the initial scenario. This phenomenon implies that the avian population's greater spatial mobility may result in a faster spread of the disease to susceptible population centers, even if the transmission rate is relatively low.

The exposed compartment is a transition phase that takes place when avian populations are susceptible to disease as a result of contact with infected avian populations or environments that have been contaminated by the virus. The three simulated scenarios exhibit substantial differences in the dynamics of the exposed population as a result of the influence of epidemiological parameters and spatial movement. The simulation results depicted in Figure 4b indicate that the exposed population reached its maximum after six days following the outbreak in the initial scenario. Meanwhile, the exposed population reached its maximum in the second scenario, as illustrated in Figure 5b, following 14 days of infection. This is a consequence of a reduced transmission rate, which leads to a slower transmission process. The third scenario also exhibits distinct results in Figure 6b. This scenario demonstrates that the exposed population reached its peak in a mere 11 days, despite the fact that the $\mathcal{R}_0$ value is equal to that of the second scenario. These findings suggest that the transmission process can be accelerated by a higher diffusion coefficient. The exposed population decreases over time after the peak period has passed. The exposed avian population in the first scenario experienced a more rapid decline, diminishing within 17 days of the outbreak, as opposed to the second and third scenarios, which required 30 and 53 days, respectively. The more varied spatial distribution of exposed avian populations across the domain was the result of the higher spatial distribution of the exposed population. In contrast to the exposed scenario, which was concentrated in a specific area, this led to a more gradual decline in the curve.

The evolution profile of the infected population over time, as shown in Figure 4c, is selected with $\mathcal{R}_0 > 1$. The outbreak's initial occurrence was at $x = 2.5$ km, where the infected population was concentrated in the early stages. The wave of infection began to spread to the center of the avian flock with the highest number of susceptible populations after two days of infection. The outbreak's peak infection occurred in the vicinity of the susceptible avian flock's center after 12 days. Upon reaching this infection peak, the intensity gradually diminished. In the second scenario, the number of infected individuals reached its peak after 21 days of the outbreak and continued to decline after this peak of infection, in contrast to the first scenario with $\mathcal{R}_0 < 1$ (Figure 5c). The peak of the wave of infection in this second scenario also occurred at the center of the susceptible avian population, albeit at a slower pace than in the first scenario. This slower rate of spread also suggests that the speed of infection spread is influenced by a lower infection rate. Figure 6c also displays distinct results for the third scenario, in which the initial outbreak relocates to the susceptible avian center at $x = 0$ km. The infection wave reaches its peak after 20 days of the outbreak, despite the fact that the basic reproduction number value in this scenario is identical to that of the second scenario. In contrast to the second scenario, which has a peak infection rate, the third scenario has a significantly lower number of infections. This infection pattern indicates that the spatial movement of the susceptible population has a significant impact on the spread of infection. When the diffusion coefficient is lower, the infection wave will move towards the infected avian density center at a slower pace.

The environmental virus concentration was influenced by the virus shedding from infected avians with an average of υ due to the initial conditions. Nevertheless, variation in the dynamics of environmental infections was observed across different scenarios as a result of the transmission rate and diffusion. In the initial scenario (Refer to Figure 4d), the peak environmental virus concentration occurred at the same location as the susceptible avian flock center, but at a different time, specifically 58 days after the outbreak, with $\mathcal{R}_0 > 1$. This finding suggests that, despite the fact that the infected population had decreased by day 58, the accumulated virus could still persist in the environment as a result of virus shedding from the remaining infected population. The environmental virus concentration reached its maximum after 65 days of infection in the scenario depicted in Figure 5d, where $\mathcal{R}_0 < 1$ and low diffusion. The virus concentration reaches its maximum in the third scenario in Figure 6d with high diffusion, 53 days after the outbreak period, and is situated slightly to the right of the central area of the flock. The basic reproduction number remains the same as in the second scenario. This is due to the fact that the diffusion coefficient for the virus concentration in the environment remains constant for each scenario, which leads to a relatively narrower environmental movement of the virus. Despite the fact that the virus concentration in the third scenario is still lower than in the first and second scenarios, the virus is able to spread more rapidly over

a wider area due to the higher spatial movement of the infected avian population, resulting in a faster peak wave of concentration. The simulation results for this virus concentration typically reach their maximum after the number of infected avians has decreased. Consequently, the virus in the environment has a significantly longer persistence than the host. Consequently, environmental sources of infection have a longer transmission potential and can serve as a source of additional infection, despite the fact that the infected population has declined significantly.

Additionally, in order to offer a more thorough illustration, three-dimensional simulation results for the number of infected avians and virus concentration are presented to facilitate comprehension of the spatio-temporal dynamics model (28). These three-dimensional simulations illustrate the formation, shifting, and increase or decrease of infections over time. The initial outbreak spike at $x = 2.5$ km is the initial condition provided in the reaction-diffusion model. Three-dimensional plots for the infected population are depicted in Figure 4e (first scenario), Figure 5e (second scenario), and Figure 6e (third scenario). In the first, second, and third scenarios, the spread of infection reaches its peak at 12 days, 21 days, and 20 days into the outbreak period, respectively, as it moves toward the center of susceptible population density at $x = 0$ km. Similar dynamics are observed in the number of virus concentrations in the environment, as illustrated in Figure 4f (first scenario), Figure 5f (second scenario), and Figure 6f (third scenario). The virus concentration wave reaches its peak over a longer period of time than the number of infected populations. This is demonstrated by the three-dimensional plot, which appears to have a broader surface on the time axis.

The virus transmission process is significantly influenced by the free spatial movement of avian populations, as evidenced by observations. The infection can be accelerated by increasing the rate of virus transmission, while the diffusion coefficient results in a wider spread across the entire domain. It is crucial to emphasize that a specific diffusion factor can expedite spatial infection; however, the number of infected avian populations remains relatively low if the basic reproduction number is below the epidemiological threshold. In this scenario, the disease will spread to a broader area before ultimately leading to extinction, even if the transmission rate is relatively low, provided that the diffusion factor is sufficiently large.

7. Discussion

This study introduces a $SEIZ$ epidemiological model that considers influenza transmission through direct contact between birds and indirect transmission through environmental contamination. The spatial dimension is not taken into account by the classical ODE model, which is widely used. Rather, it assumes a well-mixed population. As a result, the spatial distribution of disease spread is not captured by this ODE model. The ODE model fails to account for the fact that disease transmission is a spatially mediated process. Consequently, this model incorporates diffusion factors into the $SEIZ$ framework to investigate the transmission of infection associated with the spatial migration of avian hosts. The reaction-diffusion model is improved by Neumann boundary conditions, which are characterized as isolated domains with Gaussian-distributed spikes representing the initial outbreak conditions. Even when the basic reproduction number is below the epidemiological threshold, numerical simulations demonstrate that spatial movement is essential for the transmission of influenza infection among avian hosts.

Simulations indicate that even with $\mathcal{R}_0 < 1$, disease transmission may persist due to spatial mobility, enabling the infection to infiltrate regions with the highest concentration of susceptible individuals before ultimately vanishing. An elevated diffusion coefficient may expedite the propagation of the disease wave, albeit potentially resulting in a diminished peak wave of disease. Enhancing the impact of spatial diffusion in the model can expand the geographic range of virus transmission. The infection process will attain a prolonged peak wave when $\mathcal{R}_0 < 1$ in contrast to when the basic reproduction number exceeds the epidemiological threshold. The virus will persist in the environment longer than infected birds, creating potential future transmission sources. The findings indicate that halting the dissemination of the influenza virus requires attention not only to epidemiological parameters but also to the mobility of avians, necessitating the restriction of avian movement through the utilization of natural conditions or existing technology. This study aligns with the research presented by [40] and [41], which underscores the significant influence of spatial factors on the epidemiological dynamics of virus transmission.

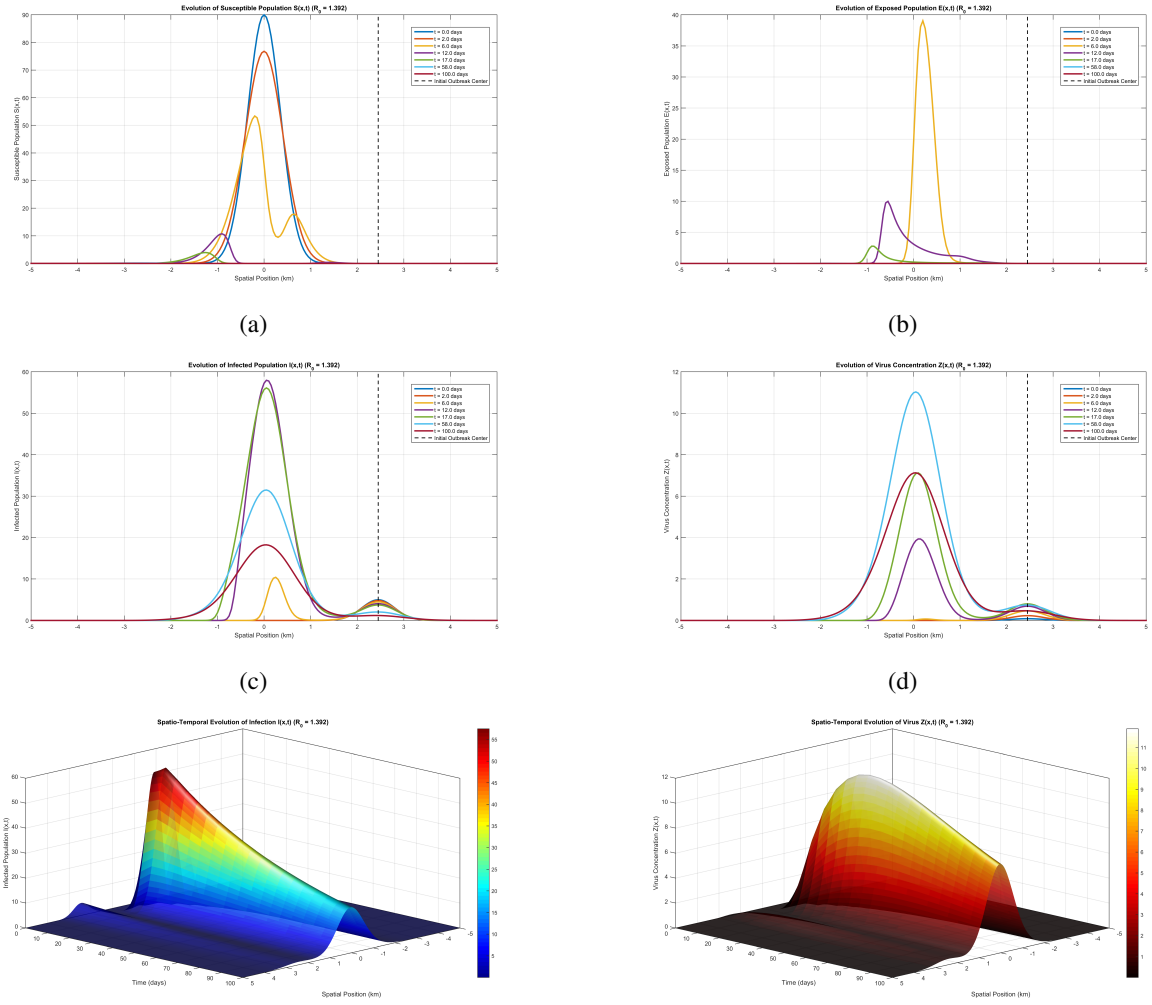

Figure 4. Spatio-temporal dynamics of Model (28) with: $\mathcal{R}_0 = 1.392$, $\pi = 0.088/365$, $\gamma = 0.45$, $\beta = 0.443$, $\mu = 0.9/90$, $\alpha = 0.52$, $\upsilon = 0.017$, $\xi = 1/19$, $I_A = 1$, $S_0 = 90$, $I_0 = 5$, $\kappa = 0.8$, $S_{\text{ext}} = 2$, $D_s = 0.01$, $D_e = D_i = D_z = 0.001$. **(a)** Susceptible Population, **(b)** Exposed Population, **(c)** Infected Population, **(d)** The Virus Particles. Scenario 1: Infection disseminates swiftly within a confined region exhibiting the greatest concentration of infected individuals. In this scenario, the quantity of viral particles may endure for a longer duration than the count of infected individuals.

This research offers a unique perspective on the significant impact of spatial diffusion on the transmission of influenza viruses, as well as qualitative information regarding the mechanisms of transmission. It can also serve as a guide for the establishment of infection quarantine zones, which prevent the transmission of infection to humans or other animals by utilizing a variety of man-made or natural barriers that are inaccessible to avian populations. Nevertheless, it is imperative to recognize the numerous constraints of this investigation. The reaction-diffusion model is constructed with a one-dimensional domain and assumes homogeneous diffusion. Consequently, the model is unable to accurately represent environmental heterogeneity. This study does not analyze the mechanisms of recovery or the emergence of immunity in the avian population, which means that it does not illustrate the ability of a specific avian species to recover alone. The Neumann boundary conditions in this instance provided an isolation of the domain, thereby preventing in-migration that could have increased the number of susceptible or infected avian populations from outside the region. The distribution of susceptible avians is depleted due to a relatively

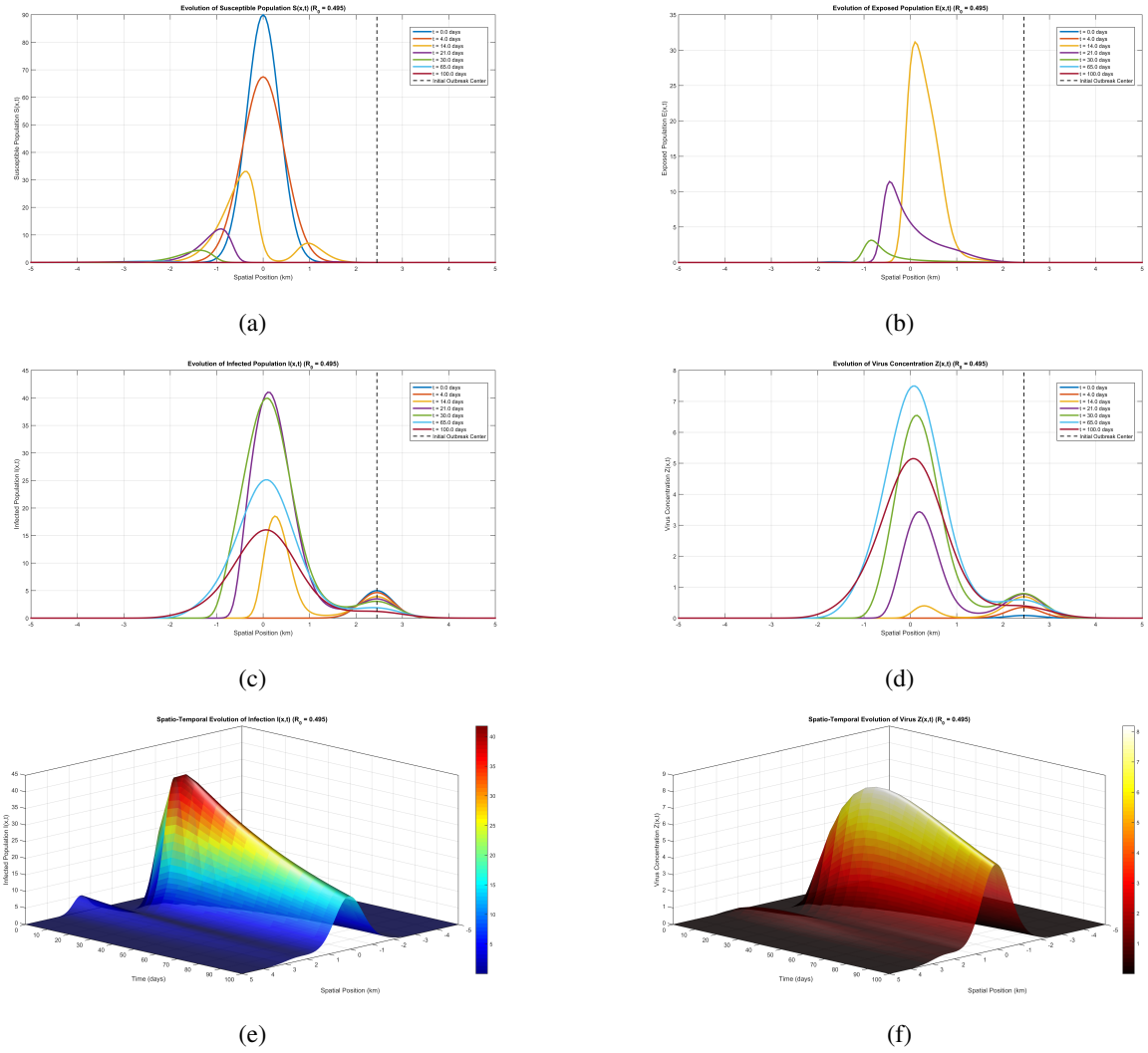

(a) (b) (c) (d) (e) (f)

Figure 5. Spatio-temporal dynamics of Model (28) with parameters: $\mathcal{R}_0 = 0.4947$, $\pi = 0.088/365$, $\gamma = 0.1$, $\beta = 0.2$, $\mu = 0.93/90$, $\alpha = 0.28$, $\upsilon = 0.017$, $\xi = 1/16$; $I_A = 1$, $S_0 = 90$, $I_0 = 5$, $\kappa = 0.8$, $S_{\text{ext}} = 2$, $D_s = 0.01$, $D_e = D_i = D_z = 0.001$.
(a) Susceptible Population, **(b)** Exposed Population, **(c)** Infected Population, **(d)** The Virus Particles. Scenario 2: Infection progresses at a slower rate in a comparatively limited region with a reduced number of infected individuals than in the first scenario.

low recruitment rate. The disease will not be maintained by the introduction of any new susceptible avians, even if $\mathcal{R}_0 > 1$. Additionally, this investigation exclusively employs local sensitivity analysis to determine the parameters that have the greatest impact on the fundamental reproduction number. Because the primary objective of this study was to analyze the dynamics of the influenza model and the reaction-diffusion model that was constructed within it, rather than to conduct an in-depth sensitivity analysis, this approach was selected. In this instance, a local sensitivity analysis is adequate to determine the parameters that have the greatest impact on the basic reproduction number. The study failed to fully capture the dynamics of the model if parameter changes are excessively large, as it only attempted to analyze the effects of minor changes in epidemiological parameters on the basic reproduction number. Several enhancements are suggested for future research. By fully accounting for environmental heterogeneity, the utilization of a two-dimensional spatial domain would facilitate more realistic analysis results. Additionally, it is

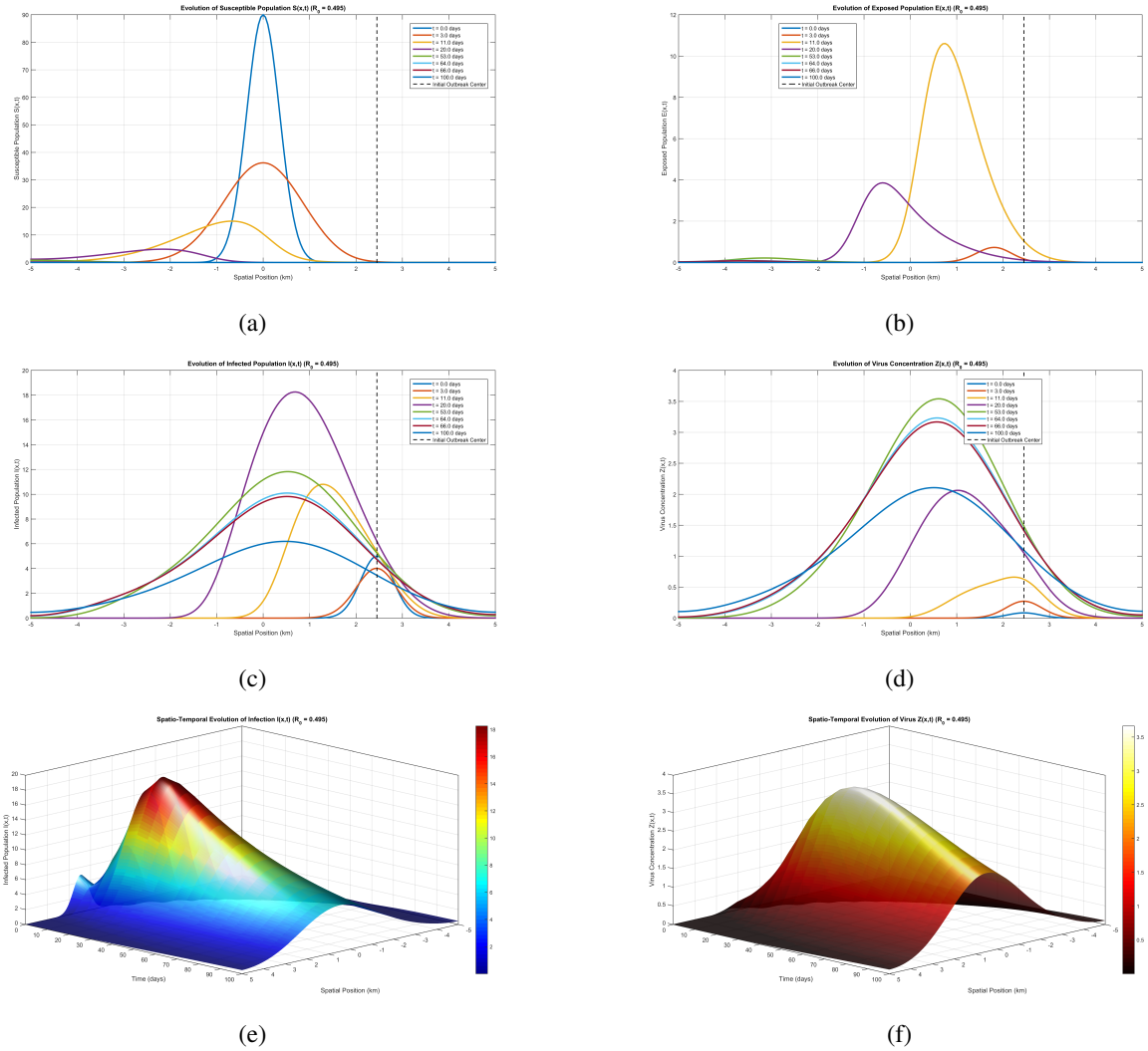

Figure 6. Spatio-temporal dynamics of Model (28) with parameters: $\mathcal{R}_0 = 0.4947$, $\pi = 0.088/365$, $\gamma = 0.1$, $\beta = 0.2$, $\mu = 0.93/90$, $\alpha = 0.28$, $\upsilon = 0.017$, $\xi = 1/16$; $I_A = 1$, $S_0 = 90$, $I_0 = 5$, $\kappa = 0.8$, $S_{\text{ext}} = 2$, $D_s = 0.1$, $D_e = D_i = 0.01$, $D_z = 0.001$.
(a) Susceptible Population, **(b)** Exposed Population, **(c)** Infected Population, **(d)** The Virus Particles. Scenario 3: Infection spreads more swiftly than in the second scenario, encompassing a larger area but involving a smaller number of infected individuals compared to the other two scenarios.

possible to incorporate parameter variations that are dependent on time in order to obtain more precise results. The epidemiological model's predictability would be enhanced by parameter estimation through field data fitting, and model validation in empirical case studies is also required for this research. Also, diffusion constants could be defined in accordance with actual data, which could result in more accurate results. Additionally, it is advised that future research include a global sensitivity analysis to facilitate the concurrent examination of each parameter space and its interactions with the model output. This development is anticipated to enhance the accuracy of the model in its support of intervention policies for the control of avian influenza.

8. Conclusion

This study expands upon the influenza virus transmission model introduced in [15] by incorporating a class of virus concentrations to establish the $SEIZ$ compartment. This study concentrates on the poultry population, excluding human and terrestrial animal populations, which are also generally susceptible to influenza infection. If $\mathcal{R}_0 < 1$, the disease-free equilibrium point will exhibit local asymptotic stability, signifying that the poultry population will remain free of disease. Disease will proliferate within avian populations as the endemic equilibrium point is locally asymptotically stable when $\mathcal{R}_0 > 1$. Sensitivity indices reveal that only the parameters μ and ξ exert a negative influence on $\mathcal{R}_0$, suggesting that augmenting these parameters may reduce the disease transmission process. Next, The influenza virus propagation model is formulated as a reaction-diffusion model with homogeneous Neumann boundary conditions, representing an isolated domain. The model undergoes numerical analysis via the Finite Volume Method, utilizing epidemic parameter values derived from prior research to yield realistic simulations. The findings of this study suggest that augmenting the diffusion constant can broaden the transmission's geographical scope, whereas elevating the basic reproduction number will expedite the onset of infection. Moreover, the virus generated by infected avian strains will exhibit a prolonged persistence relative to its host. The findings of this study suggest that intervention strategies for avian influenza transmission are inadequate if they solely address infections from bird contact; they must also incorporate measures to restrict spatial movement through technology or natural geographic barriers. In this instance, environmental sanitation is essential to disrupt the transmission chain and avert future widespread infections.

REFERENCES

1. NSW Health, *Avian Influenza ("bird flu") Fact Sheet - Fact Sheets*, NSW Government, 2024. [Online]. Available: https://www.health.nsw.gov.au/Infectious/factsheets/Pages/avian-influenza.aspx.
2. Centers for Disease Control and Prevention, *Bird flu: Causes and how it spreads*, Avian Influenza (Bird Flu), 2024. [Online]. Available: https://www.cdc.gov/bird-flu/virus-transmission/index.html.
3. Public Health Agency of Canada, *Avian influenza A(H5N1): Spread, prevention and risks*, Government of Canada, 2025. [Online]. Available: https://www.canada.ca/en/public-health/services/diseases/avian-influenza-h5n1/prevention-risks.html.
4. J. Nazir, R. Haumacher, A. C. Ike, and R. E. Marschang, *Persistence of avian influenza viruses in lake sediment, duck feces, and duck meat*, Applied and Environmental Microbiology, vol. 77, no. 14, pp. 4981–4985, 2011.
5. M. Fourment, A. E. Darling, and E. C. Holmes, *The impact of migratory flyways on the spread of avian influenza virus in North America*, BMC Evolutionary Biology, vol. 17, no. 1, p. 118, 2017.
6. Q. Mao, Z. Li, Y. Li, Y. Zhang, S. Liu, X. Yin, C. Peng, R. Ma, J. Li, G. Hou, W. Jiang, and H. Liu, *H5N1 high pathogenicity avian influenza virus in migratory birds exhibiting low pathogenicity in mallards increases its risk of transmission and spread in poultry*, Veterinary Microbiology, vol. 292, p. 110038, 2024.
7. G. Zhang, B. Li, J. Raghwani, B. Vrancken, R. Jia, S. C. Hill, G. Fournié, et al., *Bidirectional movement of emerging H5N8 avian influenza viruses between Europe and Asia via migratory birds since early 2020*, Molecular Biology and Evolution, vol. 40, no. 2, p. msad019, 2023.
8. L. Damodaran, A. Jaeger, and L. H. Moncla, *Intensive transmission in wild, migratory birds drove rapid geographic dissemination and repeated spillovers of H5N1 into agriculture in North America*, bioRxiv, Cold Spring Harbor Laboratory, 2024.
9. S. Misra, *Mathematical modeling of infectious disease spread using the SIR model*, Biomedical Journal of Scientific & Technical Research, vol. 59, no. 3, 2024.
10. C. W. Kanyiri, K. Mark, and L. Luboobi, *Mathematical analysis of influenza A dynamics in the emergence of drug resistance*, Computational and Mathematical Methods in Medicine, vol. 2018, pp. 1–14, 2018.
11. J. M. Tchuenche, S. A. Khamis, F. B. Agusto, and S. C. Mpeshe, *Optimal control and sensitivity analysis of an influenza model with treatment and vaccination*, Acta Biotheoretica, vol. 59, no. 1, pp. 1–28, 2010.
12. T. Zhang and W. Wang, *Existence of traveling wave solutions for influenza model with treatment*, Journal of Mathematical Analysis and Applications, vol. 419, no. 1, pp. 469–495, 2014.
13. Z. Xu and C. Ai, *Traveling waves in a diffusive influenza epidemic model with vaccination*, Applied Mathematical Modelling, vol. 40, no. 15-16, pp. 7265–7280, 2016.
14. Z. Xu, Y. Xu, and Y. Huang, *Traveling waves for a spatial SIRI epidemic model*, Taiwanese Journal of Mathematics, vol. 23, no. 6, pp. 1483–1503, 2019.
15. M. A. Khan, M. Farhan, S. Islam, and E. Bonyah, *Modeling the transmission dynamics of avian influenza with saturation and psychological effect*, Discrete and Continuous Dynamical Systems - S, vol. 12, no. 3, pp. 455–474, 2018.
16. R. Mu and Y. Yang, *Global dynamics of an avian influenza A(H7N9) epidemic model with latent period and nonlinear recovery rate*, Computational and Mathematical Methods in Medicine, vol. 2018, pp. 1–11, 2018.
17. A. Malek and A. Hoque, *A mathematical model of avian influenza for poultry farm and its stability analysis*, Applications and Applied Mathematics: An International Journal, vol. 15, no. 2, pp. 920–942, 2020.

18. C. Tadmon, B. Tsanou, and A. F. Feukouo, *Avian–human influenza epidemic model with diffusion, nonlocal delay and spatial homogeneous environment*, Nonlinear Analysis: Real World Applications, vol. 67, p. 103615, 2022.
19. F. M. Chuma and G. G. Mwanga, *Stability analysis of equilibrium points of Newcastle disease model of village chicken in the presence of wild birds reservoir*, International Journal of Mathematical Sciences and Computing, vol. 5, no. 2, pp. 1–18, 2019.
20. J.-F. Giroux, M. Patenaude-Monette, S. G. Gilliland, G. R. Milton, G. J. Parsons, M. L. Gloutney, K. R. Mehl, et al., *Estimating population growth and recruitment rates across the range of American common eiders*, The Journal of Wildlife Management, vol. 85, no. 8, pp. 1646–1655, 2021.
21. A. M. Tucker, C. P. McGowan, B. L. Nuse, J. E. Lyons, C. T. Moore, D. R. Smith, J. A. Sweka, K. A. Anstead, A. DeRose-Wilson, and N. A. Clark, *Estimating recruitment rate and population dynamics at a migratory stopover site using an integrated population model*, Ecosphere, vol. 14, no. 2, p. e4439, 2023.
22. A. Bouma, I. Claassen, K. Natih, D. Klinkenberg, C. A. Donnelly, G. Koch, and M. van Boven, *Estimation of transmission parameters of H5N1 avian influenza virus in chickens*, PLoS Pathogens, vol. 5, no. 1, p. e1000281, 2009.
23. A. Ssematimba, S. Malladi, T. J. Hagenaars, P. J. Bonney, J. T. Weaver, K. A. Patyk, E. Spackman, D. A. Halvorson, and C. J. Cardona, *Estimating within-flock transmission rate parameter for H5N2 highly pathogenic avian influenza virus in Minnesota turkey flocks during the 2015 epizootic*, Epidemiology and Infection, vol. 147, p. e179, 2019.
24. I. Newton, *Migration mortality in birds*, Ibis, vol. 167, no. 1, pp. 106–123, 2024.
25. V. Hénaux, M. D. Samuel, and C. M. Bunck, *Model-based evaluation of highly and low pathogenic avian influenza dynamics in wild birds*, PLoS ONE, vol. 5, no. 6, p. e10997, 2010.
26. S. P. Keeler, M. S. Dalton, A. M. Cressler, R. D. Berghaus, and D. E. Stallknecht, *Abiotic factors affecting the persistence of avian influenza virus in surface waters of waterfowl habitats*, Applied and Environmental Microbiology, vol. 80, no. 9, pp. 2910–2917, 2014.
27. W. Song, F. He, Z. Deng, M. Hu, K. Fang, W. Cheng, J. Wu, et al., *Avian influenza virus dynamics in poultry and the environment: An eight-year longitudinal study in the southwestern Poyang Lake region of China*, Infectious Disease Modelling, vol. 10, no. 4, pp. 1126–1137, 2025.
28. W. N. Harrington, S. Jasmine, S. Barman, M. M. Feeroz, M. K. Hasan, S. Akhtar, T. Jeevan, et al., *Longitudinal active avian influenza surveillance in Bangladesh from 2017–2022 reveals differential IAV and H5 infection and viral burden associated with bird species, sex, and age*, Transboundary and Emerging Diseases, vol. 2024, p. 5569836, 2024.
29. Y. Zhao, B. Richardson, E. Takle, L. Chai, D. Schmitt, and H. Xin, *Airborne transmission may have played a role in the spread of 2015 highly pathogenic avian influenza outbreaks in the United States*, Scientific Reports, vol. 9, no. 1, p. 13294, 2019.
30. E. A. Germeraad, S. W. F. Ermers, T. J. Hagenaars, M. C. M. de Jong, N. Beerens, and J. L. Gonzales, *Virus shedding of avian influenza in poultry: A systematic review and meta-analysis*, Viruses, vol. 11, no. 9, p. 812, 2019.
31. G. T. Haile, P. R. Koya, and F. M. Legesse, *Sensitivity analysis of a mathematical model for malaria transmission accounting for infected ignorant humans and relapse dynamics*, Frontiers in Applied Mathematics and Statistics, vol. 10, p. 1487291, 2025.
32. A. B. Sendor, D. Weerasuriya, and A. Sapra, *Avian influenza*, in StatPearls, Treasure Island (FL): StatPearls Publishing, 2023.
33. V. Davydovych, V. Dutka, and R. Cherniha, *Reaction–diffusion equations in mathematical models arising in epidemiology*, Symmetry, vol. 15, no. 11, p. 2025, 2023.
34. G. González-Parra, C.-L. Pérez, M. Llamazares, R.-J. Villanueva, and J. Villegas-Villanueva, *Challenges in the Mathematical Modeling of the Spatial Diffusion of SARS-CoV-2 in Chile*, Mathematical Biosciences & Engineering, vol. 22, no. 1, pp. 1680–1721, Jan. 2025.
35. R. Darazirar, A. A. Mohsen, A. Khan, M. A. Alqudah, T. Abdeljawad, and R. Thinakaran, *Mathematical Exploration of a Diffusive Infection's Dynamics and Simulation*, Scientific Reports, vol. 15, Aug. 2025.
36. S.-K. Hu, J. Huo, R. Yuan, and H.-F. Huo, *Spatial Dynamics of a two-strain Epidemic Model with Nonlocal Dispersal*, Nonlinear Analysis: Real World Applications, vol. 88, p. 104460, Apr. 2026.
37. N. Pepper, L. Gerardo-Giorda, and F. Montomoli, *Meta-modeling on detailed geography for accurate prediction of invasive alien species dispersal*, Scientific Reports, vol. 9, no. 1, p. 16237, Nov. 2019.
38. H. K. Versteeg and W. Malalasekera, *An introduction to computational fluid dynamics: The finite volume method*, 2nd ed., Pearson Education Limited, Edinburgh Gate, Harlow, Essex CM20 2JE, England, 2007.
39. Z. Kowalczuk and M. S. Tatara, *Analytical 'steady-state'-based Derivation and Clarification of the Courant-Friedrichs-Lewy Condition for Pipe Flow*, Journal of Natural Gas Science and Engineering, vol. 91, p. 103953, 2021.
40. W. Wu and Z. Teng, *The periodic traveling waves in a diffusive periodic SIR epidemic model with nonlinear incidence*, Chaos, Solitons & Fractals, vol. 144, p. 110683, 2021.
41. Z. Hou, *Traveling wave solutions of a SIR epidemic model with spatio-temporal delay*, Journal of Applied Mathematics and Physics, vol. 12, no. 10, pp. 3422–3438, 2024.